A Decoupling Two-Grid Method for the Steady-State Poisson-Nernst-Planck Equations

Ying Yang [*]   Benzhuo Lu [†]   Yan Xie [‡]

Abstract

Poisson-Nernst-Planck equations are widely used to describe the electrodiffusion of ions in a solvated biomolecular system. Two kinds of two-grid finite element algorithms are proposed to decouple the steady-state Poisson-Nernst-Planck equations by coarse grid finite element approximations. Both theoretical analysis and numerical experiments show the efficiency and effectiveness of the two-grid algorithms for solving Poisson-Nernst-Planck equations.

Key words. Poisson-Nernst-Planck equations, two-grid finite element method, decoupling method, error analysis, Gummel iteration

2000 AMS subject classifications. 65N30, 92C40.

1 Introduction

Electrodiffusion plays an important role in many fields such as biological ion channels, cellular electrophysiology and semiconductors. For the biological processes, the kinetic properties of them are mainly governed by the electrodiffusion of charged molecules in aqueous solution. The numerical methods for deriving the kinetic parameters usually include discrete methods (such as Monte Carlo, Brownian dynamics and Langevin dynamics) and continuum methods. The latter is more efficient for simulating large systems and easier to be modified to include more physical functions. The electrodiffusion processes in biomolecular systems are usually described by a continuum model called Poisson-Nernst-Planck (PNP) equations, which is regarded as one of the most efficient theoretical methods for studying electrodiffusion.

The PNP equations are a coupled system of nonlinear partial differential equations consisting of the Nernst-Planck equation and the electrostatic Poisson equation. The steady-state PNP equations in the biomolecular modeling are as follows [17]:

$$
\begin{cases}
\nabla \cdot D^i \left(\nabla p^i + \beta q^i p^i \nabla \phi \right) = 0, & \text{in } \Omega_s, \ 1 \le i \le n, \\
-\nabla \cdot (\epsilon \nabla \phi) - \lambda \sum_{i=1}^{n} q^i p^i = \rho^f, & \text{in } \Omega,
\end{cases}
\tag{1.1}
$$

where ϕ is the electrostatic potential and p^i is the concentration of the i-th ion species. This model is used to describe the electrodiffusion of mobile ions in a solvated biomolecular system (see Fig. 1). Since the analytic solutions of the PNP equations only exit in very few cases for simple shape molecules, a variety of numerical methods have been proposed to solve them [6, 7, 17, 30, 39]. For example, the finite difference method has been widely used to solve the PNP equations describing electrodiffusion in biological ion channels or other transmembrane pores [2, 12, 16, 38], but the accuracy is not so high
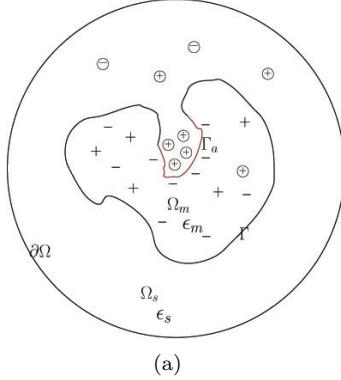
---

[*]School of Mathematics and Computing Science, Guangxi Colleges and Universities Key Laboratory of Data Analysis and Computation, Guangxi Key Laboratory of Cryptography and information Security, Guilin University of Electronic Technology, Guilin, Guangxi 541004, China. E-mail: yangying@lsec.cc.ac.cn

[†]LSEC, Institute of Computational Mathematics and Scientific/Engineering Computing, the National Center for Mathematics and Interdisciplinary Sciences, Academy of Mathematics and Systems Science, Chinese Academy of Sciences, Beijing 100190, China. E-mail: bzlu@lsec.cc.ac.cn

[‡]LSEC, Institute of Computational Mathematics and Scientific/Engineering Computing, Academy of Mathematics and Systems Science, Chinese Academy of Sciences, Beijing 100190, China

when it is applied to the biomolecular models with highly irregular surfaces. The finite element method is considered to be very promising in which irregular shapes can be fitted more easily when applying to the PNP equations. [14, 17, 18, 26, 27, 36].

(a)

Figure 1: 2-D illustration of the computational domain modeling a solvated biomolecular system. The domain $\Omega_m \subset \Omega$ represents the biomolecule(s) and the remain domain $\Omega_s = \Omega \setminus \bar{\Omega}_m$ shows a solvent surrounding the biomolecule(s). The molecular surface Γ interfaces domains Ω_m and Ω_s. Charged ligands in this model are also treated as diffusive species, and might react with the biomolecules on a part of the molecular surface Γ_a. The diffusive particles are distributed in Ω_s.

In general, there are two types of approaches to solve such a multimodel problem like PNP equations. One is to consider the equations as a large system and solve the overall system together. The other is to first decouple the system and then solve the equations respectively. The advantages of the latter are obvious. For example, it can be implemented more easily and efficiently since the computational systems are smaller; it can effectively exploit the existing computing softwares and it can result in parallelism in some cases. The Gummel iteration [11] is such a type of decoupling approach which may be the most commonly used decoupling method for solving PNP equations [3, 13, 19]. This approach is to solve one of the equations first and then substitute the solution in successive equations. For example, consider the following system coupled by two equations

$$F_1(u_1, u_2) = 0, \quad F_2(u_1, u_2) = 0.$$

The Gummel iteration for the above system could be: given u_2^0, for $k \geq 0$, find (u_1^{k+1}, u_2^{k+1}) such that

$$F_1(u_1^{k+1}, u_2^k) = 0, \quad F_2(u_1^{k+1}, u_2^{k+1}) = 0,$$

until the error between the $(k+1)$th solution and kth solution is less than the tolerance. However, the Gummel iteration converges slowly or even diverges for PNP equations modeling complex biomoleculars such as protein and DNA. There are some other approaches to decouple multimodel problems. Most of them are based on the idea of domain decomposition [5, 9, 20, 24]. Among those approaches, the two-grid finite element method closely combines with the finite element method. The two-grid finite element method was originally proposed by Xu for the partial differential equation (PDE) to deal with the asymmetry and indefiniteness [31, 32, 33] and gradually developed for some other applications such as linearization, localization and parallelization [21, 34, 35]. Compared with the work for the single PDE as above, the primary motivation of the two-grid finite element method for the coupled PDEs (which involves two or more equations) is different. It can be applied to decouple the system of PDEs and has shown the efficiency and effectiveness for some coupled systems [5, 15, 22]. Jin and his coauthors [15] used the two-grid discretization method to decouple the Schrödinger equation arising from quantum mechanics. Mu and Xu [22] presented a type of decoupling method based on two-grid finite element method and applied it to solving Stoke-Darcy model for coupling fluid flow with porous media flow.

In this paper, we will use the two-grid finite element method to decouple the system of steady-state PNP equations. Since the equations are quite different from the above multimodel problems, the design

of the two-grid method could not be directly inspired from the above work and the resulting two-grid schemes are also different. We shall design two decoupling schemes by using the two-grid method. One is semi-decoupled. The other is fully decoupled and is suitable for parallelism. These schemes can provide good initial values for solving PNP equations and do not require iterations on the fine discrete grid as the Gummel iteration does, which can improve the computational efficiency and save the computational time. We also get some analysis results. The results show that if the finite element solution on the coarse grid approximates that on the fine grid well enough, then the two-grid method can achieve the similar approximation effect that the conventional finite element method could do. Some numerical examples including a biomolecular problem are shown to verify the theoretic results.

The paper is organized as follows. In the following section, some preliminaries including the introduction to the PNP equations are presented. In Section 3, two decoupling two-grid algorithms are proposed and the corresponding error analyses are presented. Some numerical examples are shown in Section 4.

2 Preliminaries

In this section, we shall first describe the steady-state PNP equations and boundary conditions, then introduce the corresponding weak formulations. The finite element approximations are also studied in this section.

In this paper, we consider the following steady-state PNP system for simulating biomolecular diffusion-reaction process [17, 36]

$$\begin{cases} \nabla \cdot D^i \left(\nabla p^i + \beta q^i p^i \nabla \phi \right) = 0, & \text{in } \Omega_s, \ 1 \le i \le n, \\ -\nabla \cdot (\epsilon \nabla \phi) - \lambda \sum_{i=1}^{n} q^i p^i = \rho^f, & \text{in } \Omega \subset R^3 \end{cases} \tag{2.1}$$

with the following interface conditions and boundary conditions (for simplicity, the reactive molecular surface Γ_a is not considered, see Fig. 1)

$$\begin{cases} [\phi]_\Gamma = 0, \ [\epsilon \frac{\partial \phi}{\partial n}]_\Gamma = 0, & \text{on } \Gamma = \bar{\Omega}_s \bigcap \bar{\Omega}_m, \\ n \cdot D^i \left(\nabla p^i + \beta q^i p^i \nabla \phi \right) = 0, & \text{on } \Gamma, \ 1 \le i \le n, \\ \phi = 0, & \text{on } \partial \Omega, \\ p^i = p^i_{pulk}, & \text{on } \partial \Omega, \end{cases} \tag{2.2}$$

where $p^i(x)$ is the concentration of the i-th species particle carrying charge q^i, $1 \le i \le n$, $\phi(x)$ is the electrostatic potential, $D^i(x)$ is the diffusion coefficient, the permanent (fixed) charge distribution $\rho^f(x) = \sum_{j=1}^{N_m} q_j \delta(x - x_j)$ is a linear combination of Dirac Delta functions and represents an ensemble of singular charges q_j located at x_j inside biomolecules, $\beta = 1/(\kappa_B T)$ is the inverse Boltzmann energy, $\epsilon(x) = \begin{cases} \epsilon_m, & x \in \Omega_m, \\ \epsilon_s, & x \in \Omega_s, \end{cases}$ is the dielectric coefficient, $\lambda = \begin{cases} 0, & \text{in } \Omega_m, \\ 1, & \text{in } \Omega_s \end{cases}$, n is the outer normal vector and p^i_{pulk}, $i = 1, 2 \cdots, n$ are given functions.

Let $\Omega \subset \mathbb{R}^3$ be a polyhedral convex domain with a Lipschitz-continuous boundary $\partial \Omega$. Assume the interface Γ is sufficiently smooth, say, of class C^2. We shall adopt the standard notations for Sobolev spaces $W^{s,p}(\Omega)$ and their associated norms and seminorms, see, e.g., [1, 4]. For $p = 2$, we denote $H^s(\Omega) = W^{s,2}(\Omega)$ and $H_0^1(\Omega) = \{v | v \in H^1(\Omega) : v |_{\partial \Omega} = 0\}$, where $v |_{\partial \Omega} = 0$ is in the sense of trace, $\| \cdot \|_{s,p,\Omega} = \| \cdot \|_{W^{s,p}(\Omega)}$ and $(\cdot, \cdot)$ is the standard L^2-inner product. The weak formulations of (2.1) and (2.2) are that: Find $\phi \in H^1(\Omega_s)$ and $p^i \in V = \{v | v \in H^1(\Omega_s), v|_{\partial \Omega} = p^i_{pulk}\}$ $(1 \le i \le n)$ such that [36]

$$a_1(p^i, v) + b_1(p^i, \phi, v) = 0, \quad \forall v \in V_0, \tag{2.3}$$

$$a_2(\phi, w) + b_2(p^i, w) = f(w), \quad \forall w \in C_0^\infty(\Omega), \tag{2.4}$$

3

where

$$a_1(p^i, v) = (D^i \nabla p^i, \nabla v), \quad b_1(p^i, \phi, v) = (D^i \beta q^i p^i \nabla \phi, \nabla v), \quad (2.5)$$

$$a_2(\phi, w) = (\epsilon \nabla \phi, \nabla w), \quad b_2(p^i, w) = (-\lambda \sum_{i=1}^{n} q^i p^i, w), \quad f(w) = (\rho^f, w), \quad (2.6)$$

and the space $V_0 = \{v | v \in H^1(\Omega_s), v|_{\partial\Omega} = 0\}$. Here $D^i(x) \geq D_0 > 0$, $\epsilon(x)$, β, $D^i(x)$ and $q^i \in L^\infty(\Omega)$, $(1 \leq i \leq n)$.

Assume that $T^h(\Omega)$ is a quasi-uniform mesh of size $h \ll 1$. For ease of analysis, we suppose that the triangulation resolves the interface, although this assumption may be weakened in the practical computation. We define linear finite element spaces

$$S^h(\Omega) = \{v \in H^1(\Omega) : v|_e \in P^1(e), \forall e \in T^h(\Omega)\}, \quad S_0^h(\Omega) = S^h(\Omega) \cap H_0^1(\Omega), \quad (2.7)$$

where $P^1(e)$ is the set of linear polynomials. The coarse spaces $S^H(\Omega)$ and $S_0^H(\Omega)$ are defined by replacing h with H in (2.7).

Suppose there exists a unique solution (ϕ, p^i) satisfying (2.3)-(2.6). The standard finite element discrete scheme for (2.3)-(2.6) reads:

Algorithm 2.1. *(Standard finite element method [36]) Find $\phi_h \in S_0^h(\Omega)$ and $p_h^i \in S^h(\Omega_s) \cap V$, $(1 \leq i \leq n)$, such that*

$$a_1(p_h^i, v_h) + b_1(p_h^i, \phi_h, v_h) = 0, \quad \forall v_h \in V_0 \cap S^h(\Omega_s), \quad 1 \leq i \leq n, \quad (2.8)$$

$$a_2(\phi_h, w_h) + b_2(p_h^i, w_h) = \hat{f}(w_h), \quad \forall w_h \in S_0^h(\Omega), \quad (2.9)$$

where $\hat{f}(w_h) = \sum_{j=1}^{N_m} q_j w_h(x_j)$ is an approximation to the functional $f(w)$ [37].

We assume there exists a unique solution (ϕ_h, p_h^i) satisfying (2.8) and (2.9). Some error bounds were presented in [36] for the finite element approximation. For example, if $\phi \in H^{1+m}(\Omega_s)$ and $p^i \in H^{1+m}(\Omega_s)$ $(1 \leq i \leq n)$, $0 < m \leq 1$, then we have

$$\|\phi - \phi_h\|_{1,\Omega_s} \leq C(h^m + \sum_{i=1}^{n} \|p^i - p_h^i\|_{0,\Omega_s}), \quad (2.10)$$

and

$$\|p^i - p_h^i\|_{1,\Omega_s} \leq C(h^m + \sum_{i=1}^{n} \|p^i - p_h^i\|_{0,\Omega_s}), \quad (2.11)$$

when $p_h^i \in L^\infty(\Omega_s)$. Although there is no error estimate in L^2 norm for the solution p_h^i of the steady-state PNP equations, the numerical results show that the second order accuracy could be achieved (see [36] and also the results in Table 2 of Section 4 in this paper).

We also note that the wellposedness and error estimations in H^1 and L^2 norms of the finite element approximation for the time-dependent PNP are presented in [23] and [28], respectively.

We introduce the auxiliary problem which shall be used in the next section: Find $w \in H^1(\Omega_s)$, such that

$$a_1(v, w) + b_1(v, \phi, w) = (f, v), \quad \forall v \in H_0^1(\Omega_s), \quad (2.12)$$

where $f \in L^2(\Omega_s)$. The finite element discrete scheme for (2.12) reads: Find $w_h \in S^h(\Omega_s)$, such that

$$a_1(v_h, w_h) + b_1(v_h, \phi, w_h) = (f, v_h), \quad \forall v_h \in S_0^h(\Omega_s). \quad (2.13)$$

Lemma 2.1. *If there exists a unique solution for the problem (2.12) when* $f \in L^2(\Omega_s)$, *then the following regularity result holds (cf. Grisvard [10])*

$$\|w\|_{2,\Omega_s} \le C\|f\|_{0,\Omega_s}.$$

Furthermore, if $\phi \in W^{2,\infty}(\Omega_s)$, *then (cf. Xu [34])*

$$\|\nabla w_h\|_{0,\Omega_s} \le C\|\nabla w\|_{0,\Omega_s}.$$

3 The two-grid finite element method

In this section, we shall present the two-grid finite element method for the PNP equations. Two algorithms are provided to decouple the strong coupled equations. The first one is a semi-decoupling scheme. The second one is a fully decoupling scheme, which is suitable for parallel computing. Some error analyses are also derived for the two-grid finite element approximations.

Algorithm 3.1. *(Two-grid algorithm I)*
Step 1. Solve the coupled problem on the coarse grid: find $p_H^i \in S^H(\Omega_s) \cap V$ $(1 \le i \le n)$ *and* $\phi_H \in S_0^H(\Omega)$, *such that*

$$a_1(p_H^i, v_H) + b_1(p_H^i, \phi_H, v_H) = 0, \quad \forall v_H \in S^H(\Omega_s) \cap V_0, \quad 1 \le i \le n, \tag{3.1}$$

$$a_2(\phi_H, w_H) + b_2(p_H^i, w_H) = \hat{f}(w_H), \quad \forall w_H \in S_0^H(\Omega), \tag{3.2}$$

where $\hat{f}(w_H) = \sum_{j=1}^{N_m} q_j w_H(x_j)$.
Step 2. We first solve the Poisson equation on the fine grid: find $\phi_h^* \in S_0^h(\Omega)$, *such that*

$$a_2(\phi_h^*, w_h) + b_2(p_H^i, w_h) = \hat{f}(w_h), \quad \forall w_h \in S_0^h(\Omega), \tag{3.3}$$

then we solve the Nernst-Planck equation on the fine grid: find $p_h^{i,*} \in S^h(\Omega_s) \cap V$, *such that*

$$a_1(p_h^{i,*}, v_h) + b_1(p_h^{i,*}, \phi_h^*, v_h) = 0, \quad \forall v_h \in S^h(\Omega_s) \cap V_0, \tag{3.4}$$

where $\hat{f}(w_h) = \sum_{j=1}^{N_m} q_j w_h(x_j)$.

Obviously, (3.1) and (3.2) in Step 1 in fact are the standard finite element discretization on a coarse space. Hence, if the Gummel iteration is applied in this step, the iteration between the coupled equations is still required but it converges faster because of much less of the degree of freedoms comparing with Algorithm 2.1. The system in Step 2 is a semi-decoupling one. To solve this system, the solution ϕ_h^* in (3.3) should be solved first and then be inserted into (3.4) to get the solution $p_h^{i,*}$. Both (3.3) and (3.4) need to be solved only for one time, respectively. Hence this algorithm could reduce plenty of computational time comparing with Algorithm 2.1 by using the Gummel iteration which requires a lot of iterations between the equations solving individually. Moreover, it can naturally avoid the slow convergence or divergence of the Gummel iteration.

The following two theorems provide the error bounds for the two-grid solutions of Algorithm 3.1 and the solutions of Algorithm 2.1.

Theorem 3.1. *If* (ϕ_h, p_h^i), (ϕ_H, p_H^i) *and* $(\phi_h^*, p_h^{i,*})$ *are the solutions of (2.8)-(2.9), (3.1)-(3.2) and (3.3)-(3.4), respectively, then*

$$\|\nabla(\phi_h - \phi_h^*)\|_{0,\Omega} \le C \sum_{i=1}^{n} \|p_h^i - p_H^i\|_{0,\Omega_s}. \tag{3.5}$$

Proof. From (2.9) and (3.3), we have

$$a_2(\phi_h - \phi_h^*, w_h) + b_2(p_h^i - p_H^i, w_h) = 0, \quad \forall w_h \in S_0^h(\Omega).$$

Taking $w_h = \phi_h - \phi_h^*$ in the above equality, we obtain

$$
\begin{aligned}
\|\nabla(\phi_h - \phi_h^*)\|_{0,\Omega}^2 &\leq |a_2(\phi_h - \phi_h^*, \phi_h - \phi_h^*)| \\
&= |b_2(p_h^i - p_H^i, \phi_h - \phi_h^*)| \\
&\leq \sum_{i=1}^n \|p_h^i - p_H^i\|_{0,\Omega_s} \|\phi_h - \phi_h^*\|_{0,\Omega_s}.
\end{aligned}
$$

Hence,

$$\|\nabla(\phi_h - \phi_h^*)\|_{0,\Omega} \leq C \sum_{i=1}^n \|p_h^i - p_H^i\|_{0,\Omega_s}.$$

This completes the proof. $\qquad\square$

The following error bounds in L^2 norm will be used for presenting the error estimate for the concentration in H^1 norm.

Lemma 3.1. *Suppose the assumptions of Lemma 2.1 and Theorem 3.1 hold, $p_h^{i,*} \in L^\infty(\Omega_s)$, ϕ is the solution of (2.3)-(2.4) and ϕ_h approximates ϕ well enough, then we have*

$$\|p_h^i - p_h^{i,*}\|_{0,\Omega_s} \leq C \sum_{i=1}^n \|p_h^i - p_H^i\|_{0,\Omega_s}.$$

Proof. Set $e = p_h^i - p_h^{i,*}$. Let w be the solution of the following auxiliary problem:

$$a_1(v, w) + b_1(v, \phi, w) = (e, v), \quad \forall v \in H_0^1(\Omega_s),$$

and w_h be the finite element approximation to w satisfying

$$a_1(v_h, w_h) + b_1(v_h, \phi, w_h) = (e, v_h), \quad \forall v_h \in S_0^h(\Omega_s). \tag{3.6}$$

Taking $v_h = e$ in (3.6), then from (2.8) and (3.4), we have

$$
\begin{aligned}
\|e\|_{0,\Omega_s}^2 &= b_1(p_h^{i,*}, \phi_h^*, w_h) - b_1(p_h^i, \phi_h, w_h) + b_1(p_h^i - p_h^{i,*}, \phi, w_h) \\
&= b_1(p_h^{i,*}, \phi_h^* - \phi_h + \phi_h - \phi, w_h) + b_1(p_h^i, \phi - \phi_h, w_h) \\
&= b_1(p_h^{i,*}, \phi_h^* - \phi_h, w_h) + b_1(p_h^{i,*} - p_h^i, \phi_h - \phi, w_h) \\
&\leq C(\|\nabla(\phi_h - \phi_h^*)\|_{0,\Omega_s} + \|p_h^{i,*} - p_h^i\|_{0,\Omega_s} \|\nabla(\phi - \phi_h)\|_{0,\infty,\Omega_s}) \|\nabla w_h\|_{0,\Omega_s}, \tag{3.7}
\end{aligned}
$$

where the assumption $p_h^{i,*} \in L^\infty(\Omega_s)$ is used. From Theorem 3.1 and Lemma 2.1, we get

$$\|e\|_{0,\Omega_s}^2 \leq C\left(\sum_{i=1}^n \|p_h^i - p_H^i\|_{0,\Omega_s} + \|e\|_{0,\Omega_s} \|\nabla(\phi - \phi_h)\|_{0,\infty,\Omega_s}\right) \|e\|_{0,\Omega_s}.$$

If ϕ_h approximates ϕ well enough satisfying $C\|\nabla(\phi - \phi_h)\|_{0,\infty,\Omega_s} < 1$, then we can easily get the result of Lemma 3.1. $\qquad\square$

Theorem 3.2. *Suppose the assumptions of Lemma 3.1 hold and $\phi_h \in W^{1,\infty}(\Omega_s)$, then we have*

$$\|\nabla(p_h^i - p_h^{i,*})\|_{0,\Omega_s} \leq C \sum_{i=1}^n \|p_h^i - p_H^i\|_{0,\Omega_s}.$$

Proof. Similarly, set $e = p_h^i - p_h^{i,*}$. From (2.8) and (3.4), we have

$$a_1(e, v_h) + b_1(p_h^i, \phi_h, v_h) - b_1(p_h^{i,*}, \phi_h^*, v_h) = 0, \quad \forall v_h \in S^h(\Omega_s) \cap V_0.$$

$$
\begin{aligned}
\|\nabla e\|_{0,\Omega_s}^2 &\leq C|a_1(e, e)| \\
&= C|b_1(p_h^i, \phi_h, e) - b_1(p_h^{i,*}, \phi_h^*, e)| \\
&\leq C\|p_h^i \nabla \phi_h - p_h^{i,*} \nabla \phi_h^*\|_{0,\Omega_s} \|\nabla e\|_{0,\Omega_s}.
\end{aligned}
\tag{3.8}
$$

If $p_h^{i,*} \in L^\infty(\Omega_s)$ and $\phi_h \in W^{1,\infty}(\Omega_s)$, then

$$
\begin{aligned}
\|p_h^i \nabla \phi_h - p_h^{i,*} \nabla \phi_h^*\|_{0,\Omega_s} &= \|(p_h^i - p_h^{i,*}) \nabla \phi_h + p_h^{i,*}(\nabla \phi_h - \nabla \phi_h^*)\|_{0,\Omega_s} \\
&\leq \|e\|_{0,\Omega_s} + \|\nabla \phi_h - \nabla \phi_h^*\|_{0,\Omega_s}.
\end{aligned}
\tag{3.9}
$$

Inserting (3.9) into (3.8) and using Theorem 3.1 and Lemma 3.1, we can get the result of Theorem 3.2.□

Remark 3.1. *Theorem 3.1 and Theorem 3.2 show that the errors between the finite element solution (ϕ_h, p_h^i) in Algorithm 2.1 and the two-grid solution $(\phi_h^*, p_h^{i,*})$ in Algorithm 3.1 are controlled by the error of the solution for the concentration on the coarse grid and on the fine grid. If the concentration on the coarse grid approximates to that on the fine grid well enough, for example,*

$$\sum_{i=1}^{n} \|p_h^i - p_H^i\|_{0,\Omega_s} = O(H^2),$$

then from Theorem 3.1 and Theorem 3.2 we have

$$\|\nabla(\phi_h - \phi_h^*)\|_{0,\Omega} = O(H^2) = O(h) \tag{3.10}$$

and

$$\|\nabla(p_h^i - p_h^{i,*})\|_{0,\Omega_s} = O(H^2) = O(h), \tag{3.11}$$

when $h = H^2$. This means the two-grid method can achieve the similar effect as the classic finite element method could do (since the optimal convergence rate for classic finite element method in H^1 norm is not better than $O(h)$, cf. (2.10) and (2.11)), if the solution for the concentration on the coarse grid approximates that on the fine grid well enough.

Next, we shall present a fully decoupling two-grid algorithm.

Algorithm 3.2. *(Two-grid algorithm II)*
Step 1. Solve the coupled problem on the coarse grid: find $p_H^i \in S^H(\Omega_s) \cap V$ $(1 \leq i \leq n)$ and $\phi_H \in S_0^H(\Omega)$, such that

$$a_1(p_H^i, v_H) + b_1(p_H^i, \phi_H, v_H) = 0, \quad \forall v_H \in S^H(\Omega_s) \cap V_0, \quad 1 \leq i \leq n,$$

$$a_2(\phi_H, w_H) + b_2(p_H^i, w_H) = \hat{f}(w_H), \quad \forall w_H \in S_0^H(\Omega).$$

Step 2. Solve the Nernst-Planck equation and Poisson equation: find $p_h^{i,*} \in S^h(\Omega_s) \cap V$ $(1 \leq i \leq n)$ and $\phi_h^* \in S_0^h(\Omega)$, such that

$$a_1(p_h^{i,*}, v_h) + b_1(p_h^{i,*}, \phi_H, v_h) = 0, \quad \forall v_h \in S^h(\Omega_s) \cap V_0, \quad 1 \leq i \leq n, \tag{3.12}$$

$$a_2(\phi_h^*, w_h) + b_2(p_H^i, w_h) = \hat{f}(w_h), \quad \forall w_h \in S_0^h(\Omega). \tag{3.13}$$

In this algorithm, two coarse grid finite element approximations ϕ_H and p_H^i are used to decouple the system on the fine space, which is different from the case in Algorithm 3.1. The system (3.12)-(3.13) are fully decoupled, so it can be solved in parallel on the fine grid level.

The following are the error analysis for Algorithm 3.2. First, for Algorithm 3.2, we have

Theorem 3.3. *If (ϕ_h, p_h^i), (ϕ_H, p_H^i) and $(\phi_h^*, p_h^{i,*})$ are the solutions of (2.8)-(2.9), (3.1)-(3.2) and (3.12)-(3.13), respectively, then*

$$\|\nabla(\phi_h - \phi_h^*)\|_{0,\Omega} \leq C \sum_{i=1}^{n} \|p_h^i - p_H^i\|_{0,\Omega_s}. \tag{3.14}$$

The proof is the same as Theorem 3.1, since the only difference between Algorithm 3.1 and 3.2 is (3.12) which is not used in this proof.

Lemma 3.2. *Suppose the assumptions of Lemma 2.1 and Theorem 3.3 hold, $p_h^{i,*} \in L^\infty(\Omega_s)$, ϕ is the solution of (2.3)-(2.4) and ϕ_h approximates ϕ well enough, then we have*

$$\|p_h^i - p_h^{i,*}\|_{0,\Omega_s} \leq C\|\nabla\phi_h - \nabla\phi_H\|_{0,\Omega_s}.$$

Proof. The proof is similar to that of Lemma 3.1. Let $e = p_h^i - p_h^{i,*}$. From (2.8) and (3.12), we have

$$a_1(e, w_h) = b_1(p_h^{i,*}, \phi_H, w_h) - b_1(p_h^i, \phi_h, w_h).$$

Taking $e = p_h^i - p_h^{i,*}$ in (3.6) and from the above, we deduce that

$$
\begin{aligned}
\|e\|_0^2 &= b_1(p_h^{i,*}, \phi_H, w_h) - b_1(p_h^i, \phi_h, w_h) + b_1(p_h^i - p_h^{i,*}, \phi, w_h) \\
&= b_1(p_h^{i,*}, \phi_H - \phi_h + \phi_h - \phi, w_h) + b_1(p_h^i, \phi - \phi_h, w_h) \\
&= b_1(p_h^{i,*}, \phi_H - \phi_h, w_h) + b_1(p_h^{i,*} - p_h^i, \phi_h - \phi, w_h) \\
&\leq C(\|\nabla(\phi_h - \phi_H)\|_{0,\Omega_s} + \|p_h^{i,*} - p_h^i\|_{0,\Omega_s}\|\nabla(\phi - \phi_h)\|_{0,\infty,\Omega_s})\|\nabla w_h\|_{0,\Omega_s},
\end{aligned}
$$

where the assumption $p_h^{i,*} \in L^\infty(\Omega_s)$ is used. From Lemma 2.1 and the assumption ϕ_h approximates ϕ well enough satisfying $C\|\nabla(\phi - \phi_h)\|_{0,\infty,\Omega_s} < 1$, we can obtain the result of Lemma 3.2. $\qquad\square$

Theorem 3.4. *Suppose the assumptions of Lemma 3.2 hold and $\phi_h \in W^{1,\infty}(\Omega_s)$,, then we have*

$$\|\nabla(p_h^i - p_h^{i,*})\|_{0,\Omega_s} \leq C\|\nabla\phi_h - \nabla\phi_H\|_{0,\Omega_s}.$$

Proof. Set $e = p_h^i - p_h^{i,*}$. From (2.8) and (3.12), we have

$$a_1(e, v_h) + b_1(p_h^i, \phi_h, v_h) - b_1(p_h^{i,*}, \phi_H, v_h) = 0, \quad \forall v_h \in S^h(\Omega_s) \cap V_0.$$

$$
\begin{aligned}
\|\nabla e\|_{0,\Omega_s}^2 &\leq C|a_1(e, e)| \\
&= C|b_1(p_h^i, \phi_h, e) - b_1(p_h^{i,*}, \phi_H, e)| \\
&\leq C\|p_h^i \nabla\phi_h - p_h^{i,*}\nabla\phi_H\|_{0,\Omega_s}\|\nabla e\|_{0,\Omega_s}. \tag{3.15}
\end{aligned}
$$

If $p_h^{i,*} \in L^\infty(\Omega_s)$ and $\phi_h \in W^{1,\infty}(\Omega_s)$, then

$$
\begin{aligned}
\|p_h^i \nabla\phi_h - p_h^{i,*}\nabla\phi_H\|_{0,\Omega_s} &= \|(p_h^i - p_h^{i,*})\nabla\phi_h + p_h^{i,*}(\nabla\phi_h - \nabla\phi_H)\|_{0,\Omega_s} \\
&\leq \|e\|_{0,\Omega_s} + \|\nabla\phi_h - \nabla\phi_H\|_{0,\Omega_s}. \tag{3.16}
\end{aligned}
$$

The proof of Theorem 3.4 is completed if we insert (3.16) into (3.15) and use Lemma 3.2.

Remark 3.2. *From Theorem 3.3, if $\|p^i - p_H^i\|_{0,\Omega_s} = O(H^2)$, $1 \leq i \leq n$, then $\|\nabla(\phi_h - \phi_h^*)\|_{0,\Omega_s} = O(h)$ when $H = \sqrt{h}$, which implies Algorithm 3.2 is efficient for the electrostatic potential as Algorithm 3.1. From Theorem 3.4, the two-grid solution for the density $p_h^{i,*}$ in Algorithm 3.2 can achieve the same convergence rate as the finite element solution in Algorithm 2.1 only when $H = h$ (cf. (2.10)). However, the numerical results in Section 4 show the optimal convergence rate even if $H \neq h$.*

There is also another semi-decoupling algorithm like Algorithm 3.1 as follows

Algorithm 3.3. *(Two-grid algorithm III)*
Step 1. Solve the coupled problem on the coarse grid: find $p_H^i \in S^H(\Omega_s) \cap V$ $(1 \leq i \leq n)$, $\phi_H \in S_0^H(\Omega)$, such that

$$a_1(p_H^i, v_H) + b_1(p_H^i, \phi_H, v_H) = 0, \quad \forall v_H \in S^H(\Omega_s) \cap V_0, \quad 1 \leq i \leq n,$$

$$a_2(\phi_H, w_H) + b_2(p_H^i, w_H) = \hat{f}(w_H), \quad \forall v_H \in S_0^H(\Omega).$$

Step 2. We first solve the Nernst-Planck equation on the fine grid: find $p_h^{i,*} \in S^h(\Omega_s) \cap V$ $(1 \leq i \leq n)$, such that

$$a_1(p_h^{i,*}, v_h) + b_1(p_h^{i,*}, \phi_H, v_h) = 0, \quad \forall v_h \in S^h(\Omega_s) \cap V_0, \quad 1 \leq i \leq n,$$

then we solve the Poisson equation on the fine grid: find $\phi_h^* \in S_0^h(\Omega)$, such that

$$a_2(\phi_h^*, w_h) + b_2(p_h^{i,*}, w_h) = \hat{f}(w_h), \quad \forall w_h \in S_0^h(\Omega).$$

In this algorithm, only the potential ϕ_H (not the density p_H^i compared with Algorithm 3.1) on the coarse grid is used in Step 2. Since the error analysis and computational efficiency are similar to Algorithm 3.2, we shall not cover those results in this paper for simplicity.

4 Numerical Results

In this section, we shall apply the two-grid algorithms to the steady-state PNP equations to verify several derived error estimations and illustrate the efficiency of the algorithms we proposed.

Example 4.1. *First we consider the steady-state PNP equations with smooth solutions as follows (see [28] for the time-dependent PNP equations):*

$$\begin{cases} \nabla \cdot (\nabla p^i + q^i p^i \nabla \phi) = f_i, & in \ \Omega, \quad i = 1, 2, \\ -\triangle \phi - \sum_{i=1}^{2} q^i p^i = f_3, & in \ \Omega. \end{cases}$$

Here the computational domain $\Omega = [0,1]^3 \subset R^3$ and $q^1 = 1$, $q^2 = -1$. The boundary condition and the right-hand side functions are chosen so that the exact solution (ϕ, p^1, p^2) is given by

$$\begin{cases} \phi = sin\pi x \ sin\pi y \ sin\pi z, \\ p^1 = sin2\pi x \ sin2\pi y \ sin2\pi z, \\ p^2 = sin3\pi x \ sin3\pi y \ sin3\pi z. \end{cases}$$

To implement the algorithms, the code is written in Fortran and the computation is carried out on a microcomputer. we use piecewise linear finite elements on the tetrahedral mesh to discretize the equations. For comparison of the approximation accuracy, the finite element solution of Algorithm 2.1 is solved by the following Gummel iteration: given the initial value $(p^{1,0}, p^{2,0}) \in S_0^h(\Omega) \times S_0^h(\Omega)$, for $m \geq 0$, find $(p^{1,m+1}, p^{2,m+1}, \phi^{m+1}) \in S_0^h(\Omega) \times S_0^h(\Omega) \times S_0^h(\Omega)$ such that

$$(\nabla \phi^{m+1}, \nabla w) + \sum_{i=1}^{2} q^i(p^{i,m}, w) = (f_3, w), \quad \forall w \in S_0^h(\Omega).$$

$$(\nabla p^{i,m+1}, \nabla v) + (q^i p^{i,m+1} \nabla \phi^{m+1}, \nabla v) = (f_i, v), \quad \forall v \in S_0^h(\Omega), \quad i = 1, 2.$$

The stopping criterion for this iteration is $\|\phi^{m+1} - \phi^m\|_0 < 10^{-5}$. The numerical results in Table 1 and 2 show that the convergence orders in H^1 norm and L^2 norm approximate first order and second order, respectively. The numerical results coincide with the theoretical results (see (2.10) and (2.11)).

To derive the two-grid solution of Algorithm 3.1, the above Gummel iteration is used on the coarse grid and then the decoupled system is solved on the fine grid by using the coarse grid solution, see the following steps:

Step 1. Given the initial value $(p^{1,0}, p^{2,0}) \in S_0^H(\Omega) \times S_0^H(\Omega)$, for $m \geq 0$ find $(p^{1,m+1}, p^{2,m+1}, \phi^{m+1}) \in S_0^H(\Omega) \times S_0^H(\Omega) \times S_0^H(\Omega)$ such that

$$(\nabla\phi^{m+1}, \nabla w) + \sum_{i=1}^2 q^i(p^{i,m}, w) = (f_3, w), \quad \forall w \in S_0^H(\Omega). \tag{4.17}$$

$$(\nabla p^{i,m+1}, \nabla v) + (q^i p^{i,m+1} \nabla\phi^{m+1}, \nabla v) = (f_i, v), \quad \forall v \in S_0^H(\Omega), \quad i = 1, 2. \tag{4.18}$$

Suppose p_H^i, $i = 1, 2$ is the final solution of the concentration in the above iteration.

Step 2. We first solve the Poisson equation on the fine grid: find $\phi_h^* \in S_0^h(\Omega)$, such that

$$(\nabla\phi_h^*, \nabla w_h) + \sum_{i=1}^2 q^i(p_H^i, w_h) = (f_3, w_h), \quad \forall w_h \in S_0^h(\Omega), \tag{4.19}$$

then we solve the Nernst-Planck equation on the fine grid: find $p_h^{i,*} \in S_0^h(\Omega)$, $\phi_h^* \in S_0^h(\Omega)$, such that

$$(\nabla p_h^{i,*}, \nabla v_h) + \sum_{i=1}^2 q^i(p_h^{i,*}\nabla\phi_h^*, \nabla v_h) = (f_i, v_h), \quad \forall v \in S_0^h(\Omega), \quad i = 1, 2. \tag{4.20}$$

The errors between the exact solution and the two-grid solutions of Algorithm 3.1 are shown in Table 3 with varying mesh size and $h = H^2$. The errors in H^1 norm approximate the second-order reduction as h becomes smaller, which indicates two-grid Algorithm 3.1 remains the same order of accuracy as Algorithm 2.1 but requires much less computational time than Algorithm 2.1 by comparing Table 1 with Table 3.

h	$\|\phi_h - \phi\|_1$	$\|p_h^1 - p^1\|_1$	$\|p_h^2 - p^2\|_1$	CPU(S)
1/4	9.14E-01	3.03E+00	5.39E+00	1.5
1/8	4.80E-01	1.82E+00	3.75E+00	–
1/16	2.43E-01	9.57E-01	2.10E+00	7.4
1/32	1.22E-01	4.85E-01	1.09E+00	–
1/64	6.09E-02	2.44E-01	5.47E-01	2933

Table 1: The H^1 norm errors between the exact solution and the finite element solutions of Algorithm 2.1.

h	$\|\phi_h - \phi\|_0$	$\|p_h^1 - p^1\|_0$	$\|p_h^2 - p^2\|_0$
1/4	8.97E-02	2.41E-01	3.26E-01
1/8	2.50E-02	8.99E-02	1.72E-01
1/16	6.44E-03	2.53E-02	5.59E-02
1/32	1.62E-03	6.51E-03	1.50E-02
1/64	4.06E-04	1.64E-03	3.83E-03

Table 2: The L^2 norm errors between the exact solution and the finite element solutions of Algorithm 2.1.

The two-grid solutions of Algorithm 3.2 are obtained by using the similar computational procedure in (4.17)-(4.20), but (4.20) is replaced with the following equation:

$$(\nabla p_h^{i,*}, \nabla v_h) + \sum_{i=1}^2 q^i(p_h^{i,*}\nabla\phi_H, \nabla v_h) = (f_i, v_h), \quad \forall v \in S_0^h(\Omega), \quad i = 1, 2.$$

10

H	h=H^2	$\|\phi_h^* - \phi\|_1$	$\|p_h^{1,*} - p^1\|_1$	$\|p_h^{2,*} - p^2\|_1$	CPU(S)
1/2	1/4	9.15E-01	3.03E+00	5.39E+00	1.2
1/4	1/16	2.44E-01	9.57E-01	2.10E+00	2.2
1/8	1/64	6.22E-02	2.44E-01	5.47E-01	830

Table 3: The H^1 norm errors between the exact solution and the two-grid finite element solutions of Algorithm 3.1.

The errors between the exact solution and the two-grid solutions of Algorithm 3.2 are shown in Table 4. The errors for the potential ϕ_h^* in H^1 norm approximate the second-order $O(H^2)$ reduction as H becomes smaller, but the error of the solutions $p_h^{1,*}$, $p_h^{2,*}$ can not achieve the second-order reduction, when $h = H^2$ (Comparing Table 4 with Table 1). Such an order reduction may be caused by the low order approximation for potential ϕ_H on coarse grid to ϕ_h on fine grid (See Theorem 3.4). This problem can be solved by using a smaller size of coarse grid (see the result of last row in Table 4). That means two-grid Algorithm 3.3 can also achieve the same order of accuracy as the finite element method could do, if we choose a suitable coarse mesh size H.

H	h	$\|\phi_h^* - \phi\|_1$	$\|p_h^{1,*} - p^1\|_1$	$\|p_h^{2,*} - p^2\|_1$	CPU(S)
1/2	1/4	9.15E-01	3.03E+00	5.39E+00	1.2
1/4	1/16	2.44E-01	9.89E-01	2.10E+00	2.2
1/8	1/64	6.22E-02	2.92E-01	5.70E-01	830
1/32	1/64	6.09E-02	2.46E-01	5.48E-01	1189

Table 4: The H^1 norm errors between the exact solution and the two-grid finite element solutions of Algorithm 3.2.

Example 4.2. *The second example is to solve (2.1)-(2.2) for a dialanine system within a spherical computational domain with radius of $400\mathring{A}$. We compute the potential and concentrations of the system, the molecular surface of which is schematically illustrated in Fig. 2.*
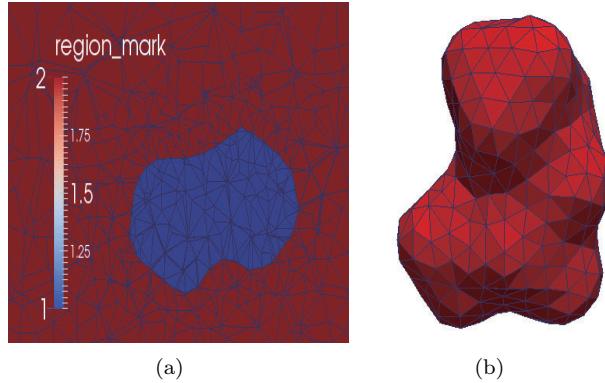

(a)   (b)

Figure 2: An example of mesh generation for the dialanine system. (a) A close-up view of the fine mesh around the molecule. region_mark = 1 denotes the solute region, region_mark = 2 denotes the solvent region. (b) The triangular boundary mesh conforming to the molecular surface.

This system carries out a fixed total charge of 0 e_c. The dielectric coefficient ϵ in (2.1) is a spacial dependent coefficient with $\epsilon_m = 2$ in the solute region and $\epsilon_s = 78$ in the solvent region. We assume that there are only monovalent ions in the salt and bulk values are set as Dirichlet conditions in the diffusion domain. We set the bulk densities in this 1:1 salt solution are $50mM$. Fig. 3 shows the distribution of the electrostatic potential and ion concentrations of the initial mesh.
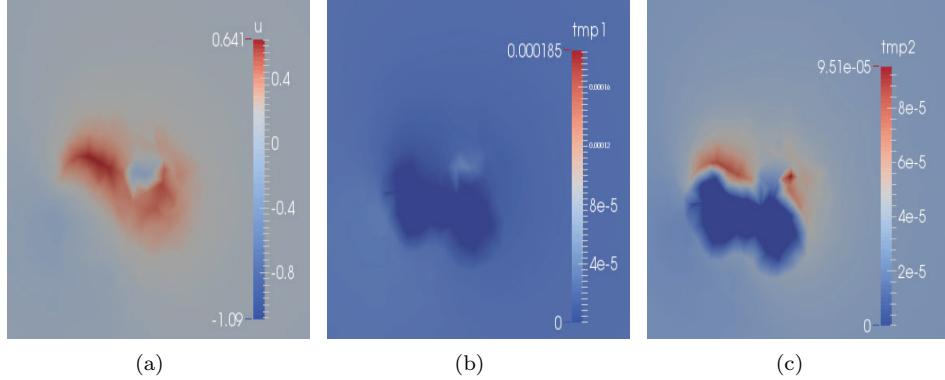
11

Figure 3: Electrostatic potential and ion density(M) around the dialanine system. (a) The potential ranges from -1.09 to 0.64 $kcal/mol \cdot e_c$. (b) Cation concentration distribution ranges from 0 to 1.85×10^{-4} (M). (c) Anion concentration distribution ranges from 0 to 9.51×10^{-5}(M).

The implementation of the algorithms is based on the parallel adaptive finite element package PHG. The parallel code is written in C and uses MPI for message passing. The computation is carried out on the cluster LSSC-III of the State Key Laboratory of Scientific and Engineering Computing of China, which consists of compute nodes with dual Intel Xeon X5550 quad-core CPUs, interconnected via DDR InfiniBand network.

Since the surface of the molecule is extremely irregular in practice, the initial mesh for the computation of PNP equations should be nonuniform with a fine mesh around the surface and a coarse mesh away from the interface. Thus in the following experiment, we illustrate the convergence rate in terms of the order of the degree of freedoms N instead of that of mesh size H. For example, if the result is $\sim \mathcal{O}(H)$, then we think it is consistent with the estimation $\sim \mathcal{O}(N^{-\frac{1}{3}})$ for this three dimensional problem. If we plot the log-log figure for the original outputs (x-axis denotes the number of N, y-axis denotes the L^2 or H^1 norm of errors), then the decay rate of the line should be $-\frac{1}{3}$. Similarly, the decay rate should be $-\frac{2}{3}$ if the result is $\sim \mathcal{O}(H^2)$. To estimate the convergence rate, we refine the initial mesh step by step and use them as coarse meshes respectively.

The numerical results for Algorithm 3.1 and 3.2 are shown in Fig. 4 and 5, respectively. It is shown from Fig. 4 that the convergence curve of $\sum_i \|p_h^i - p_h^{i,*}\|_{1,\Omega_s}$ approximates to the line with slope $-\frac{2}{3}$. This means the two-grid solution of the concentration in Algorithm 3.1 has the optimal convergence rate which coincides with our theory in Section 3 (If $\|p^i - p_h^i\|_{0,\Omega_s} = O(h^2)$, then $\sum_i \|p_h^i - p_H^i\|_{0,\Omega_s} = O(H^2)$ and from Theorem 3.2 $\sum_i \|p_h^i - p_h^{i,*}\|_{1,\Omega_s} = O(H^2)$). Moreover, the convergence curve of H^1 error for the electrostatic potential decays faster than the line with slope $-\frac{2}{3}$ presenting a superconvergence phenomenon (see (b) in Fig. 4). Similar results can be observed from Fig. 5 for Algorithm 3.2. The concentration presents an optimal convergence phenomenon in H^1 norm which indicates the theoretical result in Theorem 3.4 is not optimal. Similar to the result for Algorithm 3.1, the two-grid solution of electrostatic potential produces a numerically superconvergence phenomenon which may be caused by the good discrete mesh for this problem and requires further investigation.

5 Conclusion

In this paper, two decoupling two-grid finite element algorithms are proposed for the PNP equations. Theoretical analysis and numerical experiments show that the two-grid algorithms remain the same order of accuracy but require much less computational time compared with the classic finite element method combing with the Gummel iteration. It is promising to extend these approaches to more general settings,
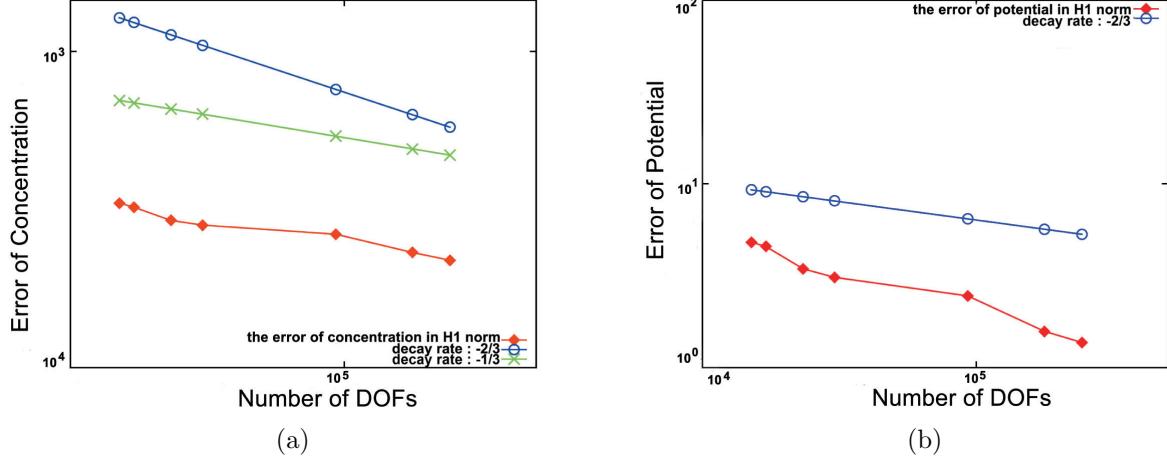
Figure 4: The error estimations of Algorithm 3.1. (a) The convergence curves of $\sum_i \|p_h^i - p_h^{i,*}\|_1$; (b) The convergence curves of $\|\phi_h - \phi_h^*\|_1$. (DOFs represents the degree of freedoms on the coarse grid.)
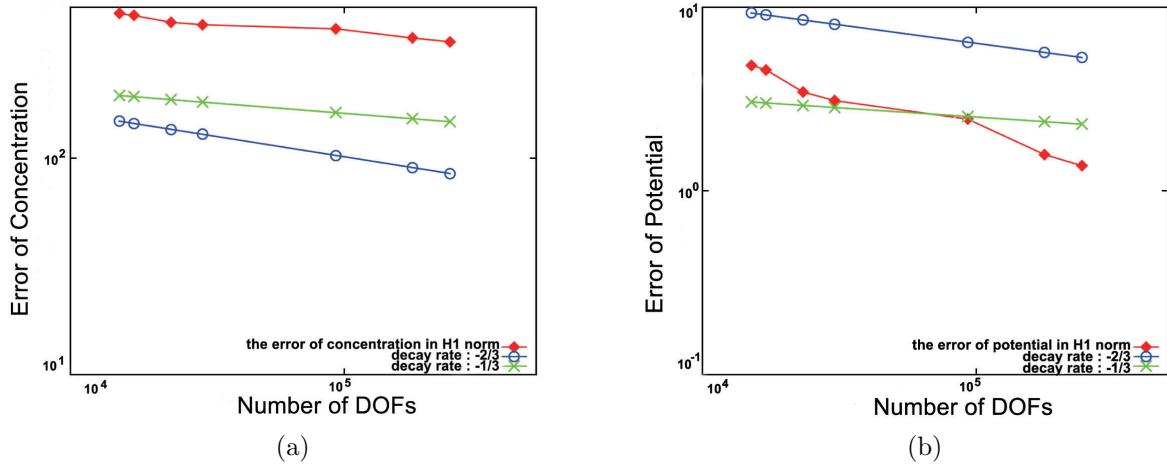

Figure 5: The error estimations of Algorithm 3.2. (a) The convergence curves of $\sum_i \|p_h^i - p_h^{i,*}\|_1$; (b) The convergence curves of $\|\phi_h - \phi_h^*\|_1$. (DOFs represents the degree of freedoms on the coarse grid.)

such as time-dependent PNP equations for ion channels, PNP equations for semiconductor devices, as well as modified PNP equations with size effects. It is also possible to generalize the framework to multilevel methods.

References

[1] R. A. Adams, Sobolev Spaces, Academic Press, New York, 1975.

[2] D. S. Bolintineanu, A. Sayyed-Ahmad, H. T. Davis, and Y. N. Kaznessis, Poisson-Nernst-Planck models of nonequilibrium ion electrodiffusion through a protegrin transmembrane pore, PLOS Comp. Bio., 5, 2009, e1000277.

[3] M. Burger, a globally convergent Gummel map for optimal dopant profiling, Math. Models Methods Appl. Sci., 19, 2011, 769-786.

[4] S. C. Brenner and L. R. Scott, The Mathematical Theory of Finite Element Methods, Springer-Verlag, New York, 1994.

[5] M. Cai, M. Mu and J. Xu, Numerical solution to a mixed Navier-Stokes/Darcy model by the two-grid approach, SIAM J. Numer. Anal., 47, 2009, 3325-3338.

[6] A. E. Cardenas, R. D. Coalson and M. G. Kurnikova, Three-dimensional Poisson-Nernst-Planck theory studies: influence of membrane electrostatics on gramicidin a channel conductance, Biophys. J., 79, 2000, 80-93.

[7] R. Eisenberg and D. P. Chen, Poisson-Nernst-Planck(PNP) theory of an open ionic channel, Biophys. J., 64 (2), 1993, A22-A22.

[8] B. Eisenberg, Y. Hyon and C. Liu, Energy variational analysis of ions in water and channels: Field theory for primitive models of complex ionic fluids, J Chem Phys., 133, 2010, 104104.

[9] R. Glowinski, T. Pan, and J. Periaux, A Lagrange multiplier/fictitious domain method for the numerical simulation of incompressible viscous flow around moving grid bodies: I. Case where the rigid body motions are known a priori, C. R. Acad. Sci. Paris Ser. I Math., 324, 1997, 361-369.

[10] E. Grisvard, Elliptic Problems in Nonsmooth Domains, Pitman, Boston, MA, 1985.

[11] H. K. Gummel, A self-consistent iterative scheme for one-dimensional steady state transistor calculations, IEEE Trans. Electron Devices, 11, 1964, 455-465.

[12] W. Im and B. Roux, Ion permeation and selectivity of OmpF porin a theoretical study based on molecular dynamics, brownian dynamics, and continuum electrodiffusion theory, J. Mol. Biol., 322, 2002, 851-869.

[13] J. W. Jerome and B. Brosowski, Evolution systems in semiconductor device modeling: A cyclic uncoupled line analysis for the gummel map, Math. Method. Appl. Sci., 9, 1987, 455-492.

[14] J. W. Jerome and T. Kerkhoven, A finite element approximation theory for the drift-diffusion semiconductor model, SIAM J. Numer. Anal., 28, 1991, 403-422.

[15] J. Jin, S. Shu and J. Xu, a two-grid discretization method for decoupling systems of partial differential equations, Math. Comp., 75, 2006, 1617-1626.

[16] M. G. Kurnikova, R. D. Coalson, P. Graf and A. Nitzan, A lattice relaxation algorithm for three-dimensional Poisson-Nernst-Planck theory with application to ion transport through the gramicidin a channel, Biophys. J., 76 (2), 1999, 642-656.

[17] B. Z. Lu, M. J. Holst, J. A. McCammo and Y. C. Zhou, Poisson-Nernst-Planck equations for simulating biomolecular diffusion-reaction processes I: finite element solutions, J. Comput. Phys., 229, 2010, 6979-6994.

[18] B. Z. lu, Y. C. Zhou, G. A. Huber, S. D. Bond, M. J. Holst and J. A. McCammon, Electrodiffusion: a continuum modeling framework for biomolecular systems with realistic spatiotemporal resolution, J. Chem. Phys., 127, 2007, 135102.

[19] B. Z. lu, Y. C. Zhou, Poisson-Nernst-Planck Equations for Simulating Biomolecular Diffusion-Reaction Processes II: Size Effects on Ionic Distributions and Diffusion-Reaction Rates, Biophys J., 100, 2011, 2475C2485.

[20] S. Markus, E. Houstis, A. Catlin, J. Rice, P. Tsompanopoulou, E. Vavalis, D. Gottfried, K. Su, and G. Balakrishnan, An agent-based netcentric framework for multidisciplinary problem solving environments (MPSE), Internat. J. Comput. Engrg. Sci., 1, 2000, 33-60.

[21] M. Marion and J. Xu, Error estimates on a new nonlinear Galerkin method based on two-grid finite elements, SIAM J. Numer. Anal., 32, 1995, 1170-1184.

[22] M. Mu and J. Xu, A two-grid method of a mixed Stoke-Darcy model for coupling fluid flow with porous media flow, SIAM J. Numer. Anal., 45, 2007, 1801-1813.

[23] A. Prohl and M. Schmuck, Convergent discretizations for the Nernst-Planck-Poisson system, Numer. Math., 111, 2009, 591-630.

[24] A. Quarteroni and A. Valli, Domain Decomposition Methods for Partial Differential Equations, Oxford University Press, Oxford, UK, 1999.

[25] A. Singer and J. Norbury, A Poisson-Nernst-Planck model for biological ion channels-an asymptotic analysis in a three-dimensional narrow funnel, SIAM J. Appl. Math., 70, 2009, 949-968.

[26] Y. H. Song, Y. J. Zhang, C. L. Bajaj, and N. A. Baker, Continuum diffusion reaction rate calculations of wild-type and mutant mouse acetylcholinesterase: adaptive finite element analysis, Biophys. J., 3, 2004, 1558-1566.

[27] Y. H. Song, Y. J. Zhang, T. Y. Shen, C. L. Bajaj, J. A. McCammon, and N. A. Baker, Finite element solution of the steady-state Smoluchowski equation for rate constant calculations, Biophys. J., 4, 2004, 2017-2029.

[28] Y. Z. Sun, P. T. Sun, B. Zheng and G. Lin, Error analysis of finite element method for Poisson-Nernst-Planck equations, J. Comput. Appl. Math., 301, 2016, 28-43.

[29] J. P. Whiteley, K. Gillow, S. J. Tavener and A. C. Walter, Error bounds on block Gauss-Seidel solutions of coupled multiphysics problems, Int. J. Numer. Meth. Engng., 88, 2011, 1219-1237.

[30] J. Wu, V. Srinivasan, J. Xu, and C. Wang, Newton-Krylov-Multigrid algorithms for battery simulation, J. Electrochem. Soc., 149, 2002, 1342-1348.

[31] J. Xu, A new class of iterative methods for nonselfadjoint or indefinite problems, SIAM J. Numer. Anal., 29, 1992, 303-319.

[32] J. Xu, A novel two-grid method for semilinear equations, SIAM J. Sci. Comput., 15, 1994, 231-237.

[33] J. Xu, Two-grid discretization techniques for linear and nonlinear PDE, SIAM J. Numer. Anal., 33, 1996, 1759-1777.

[34] J. Xu and A. Zhou, Local and parallel finite element algorithms based on two-grid discretizations, Math. Comp., 69, 1999, 881-909.

[35] J. Xu and A. Zhou, Local and parallel finite element algorithms for eigenvalue problems, Acta Mathematicae Applicatea Sinica, English Series, 18, 2002, 185-200.

[36] Y. Yang and B. Z. Lu, An Error Analysis for the Finite Element Approximation to the Steady-state Poisson-Nernst-Planck Equations, Adv. Appl. Math. Mech., 5, 2013, 113-130.

[37] Y. Yang and A. Zhou, Two-scale finite element Greens function approximations with applications to electrostatic potential computation, J. Syst. Sci. Complex., 23, 2010, 177C193.

[38] Q. Zheng, D. Chen, and G. W. Wei, Second-order poisson-nernst-planck solver for ion transport, J. Comput. Phys, 230, 2011, 5239-5262.

[39] Y. C. Zhou, B. Z. Lu, G. A. Huber, M. J. Holst and J. A. McCammon, Continuum simulations of acetylcholine consumption by acetylcholinesterase: a Poisson-Nernst-Planck approach, J. Phys. Chem. B, 112 (2), 2008, 270-275.